scientific reports

Check for updates

OPEN

Intranasal administration of a panreactive influenza antibody reveals Fc-independent mode of protection

Anna L. Beukenhorst[1,2]✉, Keira L. Rice[2], Jacopo Fralliciardi[2], Martin H. Koldijk[2], Carolyn M. Boudreau[2], Justin Crawford[2], Lisette A. H. M. Cornelissen[3], Kelly A. S. da Costa[4], Babette A. de Jong[2], Stephanie Fischinger[2], Boris Julg[2,5], Jaco M. Klap[2], Clarissa M. Koch[2], Zoltán Magyarics[2], Faez A. Nait Mohamed[5], Vintus Okonkwo[5], Lindsey Adams[5], Caitlin M. McCarthy[5], Larance Ronsard[5], Nigel Temperton[4], Helene Vietsch[2], Kanin Wichapong[6,7], Bertjan Ziere[2], Daniel Lingwood[5] & Jaap Goudsmit[1,8]

Monoclonal antibodies have two core mechanisms of protection: an antibody's antigen-binding fragment (Fab) can bind and neutralize viral pathogens and its fragment crystallizable domain (Fc) catalyzes effector functions. We investigated the relative contribution of Fab- versus Fc-mediated mechanisms of protection through passive administration of distinct forms of the pan-reactive anti-influenza antibody CR9114. We demonstrated that the contribution of Fc-independent (Fab-dependent) versus Fc-dependent mechanisms of protection is defined by the route of administration. We used CR9114 variants (wild-type, two Fc-silenced variants, or the bivalent antigen-binding fragment F(ab′)$_2$), administered either intravenously or intranasally. We found that intravenously-administered CR9114 requires the Fc domain to provide potent, pre-exposure protection against influenza A and B viral challenge. In contrast, when CR9114 was administered locally to the nasal mucosa, the main mode of protection was provided by F(ab′)$_2$, and was largely Fc-independent. Importantly, this mode of protection following intranasal administration also applied to non-neutralized influenza B strains. Moreover, intranasal administration resulted in an increase in potency against influenza A/H1N1, A/H5N1, A/H3N2, B/Yam and B/Vic compared to intravenous administration up to 50-fold. These results shed new light on the application of monoclonal antibodies such as CR9114 to combat viral infection locally, and will help inform clinical strategies of pre-exposure prophylaxis. More fundamentally, this study uncovers distinct modes of protection for systemic versus intranasally-administered prophylactic antibodies.

Influenza A and B viruses cause seasonal epidemics, leading to a substantial disease burden worldwide[1]. Furthermore, influenza A viruses pose a significant zoonotic threat to humans[2]. The passive transfer of broadly-neutralizing monoclonal antibodies (mAbs) may provide simultaneous prophylactic protection against both seasonal epidemic strains and future, potentially pandemic, strains[3]. The broad reactivity of these anti-influenza mAbs stems from their ability to bind conserved epitopes within target viral proteins that are shared across various strains[4,5]. For example, the human monoclonal antibody CR9114 targets a region on the central stem of hemagglutinin (HA) that is conserved between all influenza A subtypes and both influenza B lineages and protects mice against lethal challenge with seasonal influenza strains H1, H3, and B as well as zoonotic strains like H2 and H5[6–8].

Neutralization by immunoglobulin G (IgG) is a traditional metric of humoral immunity and a mechanism of protection of antibodies[4,6,9–12]; however, the effector functions organized by the antibody fragment crystallizable

[1]Department of Epidemiology, Harvard T.H. Chan School of Public Health, Boston, MA, USA. [2]Leyden Laboratories, Leiden, The Netherlands. [3]Wageningen Bioveterinary Research, Wageningen University & Research, Lelystad, The Netherlands. [4]Viral Pseudotype Unit, Medway School of Pharmacy, University of Kent and University of Greenwich, Chatham, UK. [5]The Ragon Institute of Mass General, MIT and Harvard, Cambridge, MA, USA. [6]Department of Biochemistry, Cardiovascular Research Institute Maastricht (CARIM), Maastricht University, Maastricht, The Netherlands. [7]Hillmark B.V., Maastricht, The Netherlands. [8]Department of Immunology and Infectious Diseases, Harvard T.H. Chan School of Public Health, Boston, MA, USA. ✉email: anna.beukenhorst@leydenlabs.com

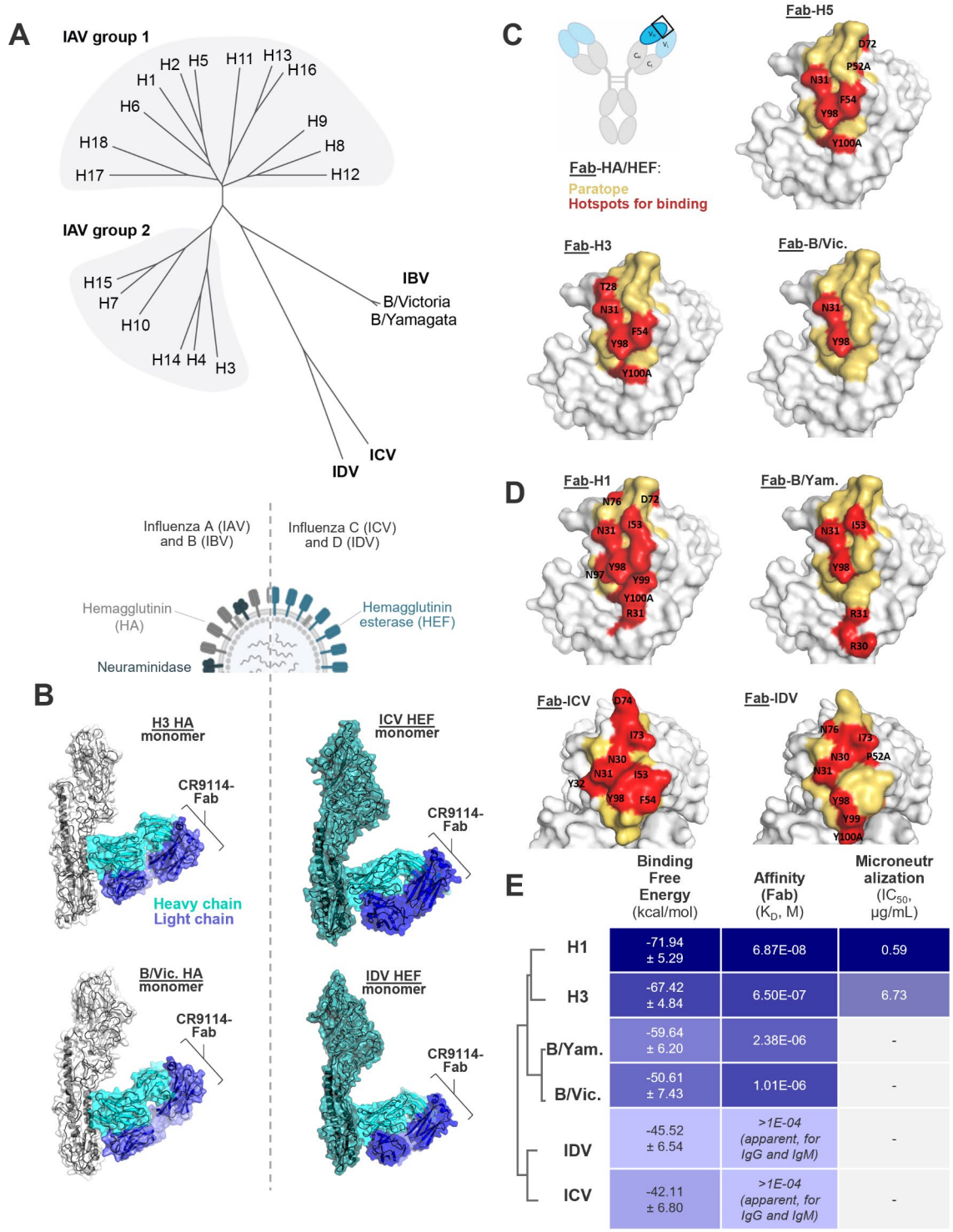

domain (Fc) are increasingly recognized as a source of immune protection in vivo[13–15]. The Fc domain of the antibody interacts with Fcγ receptors (FcγRs) that are dynamically regulated on diverse immune cell subtypes to coordinate a broad range of innate and adaptive immune reactions[16,17]. Indeed, Fc-dependent protection is widely described for antibodies with broad anti-viral target specificities, including pan-neutralizing influenza antibodies that engage invariant features of the viral spike glycoprotein hemagglutinin (HA)[4,15,18–20]. For example, intravenous CR9114 requires Fc effector functions (but not complement pathway activation) for protection of mice in vivo against lethal challenge with a non-neutralized A/H2N2 strain[8]. Whether the Fc domain of an antibody is required for protection may depend on the location of the epitope[21], the ability to neutralize influenza virus *in vitro*[8,22], and its ability to protect through other mechanisms like neuraminidase inhibition by steric hindrance[23].

◀**Fig. 1**. Pan-recognition characterization of the anti-hemagglutinin stem antibody CR9114. (**A**) Dendrogram of all known hemagglutinin (HA) subtypes and hemagglutinin esterase fusion proteins (HEF) belonging to four genera of influenza viruses: influenza A (group 1 and group 2; IAV), influenza B (Yamagata and Victoria lineages; IBV), influenza C (ICV) and influenza D (IDV). (**B**) 3D structures of CR9114 Fab in complex with H3 and B/Vic HA, and in silico models for CR9114 Fab in complex with ICV HEF and IDV HEF. (**C**) Surface representation of the CR9114-Fab paratope (yellow) and residues on CR9114-Fab that constitute binding hotspots (red) with H5, H3, and B/Vic HA. (**D**) In silico models of the CR9114-Fab paratope (yellow) that constitute binding hotspots (red) with H1 and B/Yam HA, as well as ICV and IDV HEF. (**E**) Binding Free Energy (kcal/mol), binding affinity (K_D, M), and live virus and pseudotyped virus microneutralization potency (IC_{50}, μg/mL) of CR9114 against H1, H3, B/Yamagata and B/Victoria HA, as well as ICV and IDV HEF (- : not neutralized). Affinity measurement experiments were performed with CR9114 Fab, IgG, IgM, IgA, and dIgA formats. Only the affinity for Fab is shown here, while the affinity for the other formats is presented in Fig. S2. IC_{50}s derived from the live virus neutralization assay represent four technical replicates.

The role of Fc-dependent protection has been experimentally defined in mice by passive antibody transfer followed by viral challenge, wherein the host FcγRs are genetically ablated or the transferred antibodies harbor Fc-disrupting mutations[21,24–27]. This work suggested that Fc-dependent immunity provides protection when the circulating immunoglobulin concentration is below the effective titer needed for neutralization. However, passive transfer of the neutralizing HA stem antibody MEDI8852 has also been shown to provide Fc-independent protection against sublethal challenge of non-human primates with influenza A/H5N1[28].

We sought to add to this work by simultaneously manipulating two parameters of passive antibody transfer in mice: (1) the route of administration, *i.e.*, intravenous injection or intranasal administration, to modulate antibody concentration at the site of infection; and (2) molecular configuration of the IgG (wild-type IgG, IgG-Fc-mutants, or $F(ab')_2$ bivalent antigen binding site only) to control ligation of FcγRs, investigating pre-exposure protection against neutralized and non-neutralized influenza strains.

Results

In vitro pan-influenza characteristics of the anti-hemagglutinin stem antibody CR9114

In this study, we used the human mAb CR9114, which binds all known influenza A subtypes and both influenza B lineages that cause influenza in humans and animals[6–8]. CR9114 targets the conserved central stem region on the surface membrane fusion glycoprotein hemagglutinin (HA) of influenza A and B viruses (Fig. 1A,B, and Fig. S1). It uses residues on three heavy chain complementary determining regions (HCDR1-3) and one framework region (FR3), which form flexible loops that can flip into the hydrophobic groove on HA or have polar side chains that can form H-bonds with a variety of influenza HAs. The polar side chain of tyrosine residues ^{98}YYYY^{100A} is crucial for forming H-bonds with H5 (residues on CR9114: Y^{98}, Y^{100A}), H3 (Y^{98}, Y^{100A}), and B/Vic (Y^{98}; Fig. 1C, Table S1)[23]. For influenza H1 and B/Yam, no crystal structures in complex with CR9114 are available, but molecular dynamics simulations show a key role for the same tyrosine residues of CR9114 for interacting with H1 (Y^{98}, Y^{99}, Y^{100A}) and B/Yam (Y^{98}; Fig. 1B,D, Table S1). The residues W21 and Q42 in the hydrophobic groove of HA, and D19 on the fusion peptide domain are conserved between influenza group A1 and A2 viruses and form H-bonds with CR9114 residues. CR9114 demonstrates a greater propensity to form hydrogen bonds with the hemagglutinin of influenza A compared to influenza B. This difference is evident in higher binding free energies calculated in silico for influenza A subtypes H1 and H3 in contrast to B/Yam and B/Vic. Analysis of the binding affinity of CR9114 to H1, H3, B/Yam, and B/Vic reveals that it binds strongest to H1, followed by H3, B/Vic, and B/Yam, consistent with the results of binding free energy simulations (Fig. 1E).

Using molecular dynamics simulations, we found that hotspots for CR9114 binding are partially present in the stem regions of the functionally analogous hemagglutinin-esterase-fusion (HEF) glycoprotein from influenza C and D viruses (ICV and IDV)[29–31], potentiating wider breadth than previously thought (Fig. 1B,D,E, Table S2). While no detectable affinity for HEF by CR9114 Fab was found by bio-layer interferometry, a low apparent affinity (> 100 μM) was observed for the bivalent IgG and multivalent IgM formats of this antibody (Fig. 1E).

We also tested the neutralizing activity of CR9114 against influenza A and B viruses. CR9114 shows neutralization activity for group 1 and group 2 influenza A (H1 and H3, respectively), but not for influenza B (Fig. 1E), consistent with prior studies[6,7]. Notably, neutralizing activity against influenza B becomes detectable if the apparent affinity provided by bivalent IgG is further increased by reconfiguring CR9114 as dimeric IgA (four antigen binding sites) or as pentameric IgM (ten antigen binding sites; Fig. S2), akin to the antibody isotype-associated avidity effects previously reported for neutralization of both influenza virus[32–34] and SARS-CoV-2[35].

Furthermore, we examined the ability of these CR9114 isotypes to interfere with the catalytic activity of neuraminidase (NA), the other surface glycoprotein of influenza virus A and B. As shown previously[23,36–39], CR9114 inhibits neuraminidase activity in an enzyme-linked lectin assay (ELLA, Fig. S2); the antibody sterically hinders the active site of neuraminidase and prevents cleavage of sialic acid by N1 and N2, and B/Yam NA. However, CR9114 IgG does not inhibit B/Vic in an ELLA. We show that avidity effects extend to neuraminidase inhibition, in which high avidity formats of CR9114 more potently inhibit NA than their IgG1 counterpart (Fig. S2). In conclusion, CR9114 is unique in its ability to bind influenza A, B, C and D viruses. As it has different mechanisms of action in vitro, it is the perfect candidate for investigating the contribution of various mechanisms of action to in vivo protection.

Dose-sparing effect of intranasal administration of CR9114 compared to intravenous administration, independent of in vitro microneutralization or neuraminidase inhibition

In mouse models, passive transfer of anti-influenza antibodies is typically performed through a peripheral, systemic injection route[6,7,11,21]. We hypothesized that relative to direct application to the respiratory mucosa, peripheral administration would lower prophylactic efficacy due to a reduced antibody concentration at the site of viral infection. To test this principle, we delivered de-escalating doses of CR9114 IgG (15–0.2 mg/kg) via intravenous injection or intranasal instillation 24 hours before challenging the animals with A/H1N1 (A/WSN/1933, Fig. 2A,B) or B/Victoria (B/Malaysia/2506/2004, Fig. 2C,D). We compared survival proportions at day 21 and change in body weight to the control groups, where animals received phosphate-buffered saline (PBS) either via intranasal or intravenous administration.

As expected, we observed a strong reduction in prophylactic efficacy against both influenza A and B strains (increased mortality and weight loss) during dose down-titrations in the intravenous but not intranasal groups:

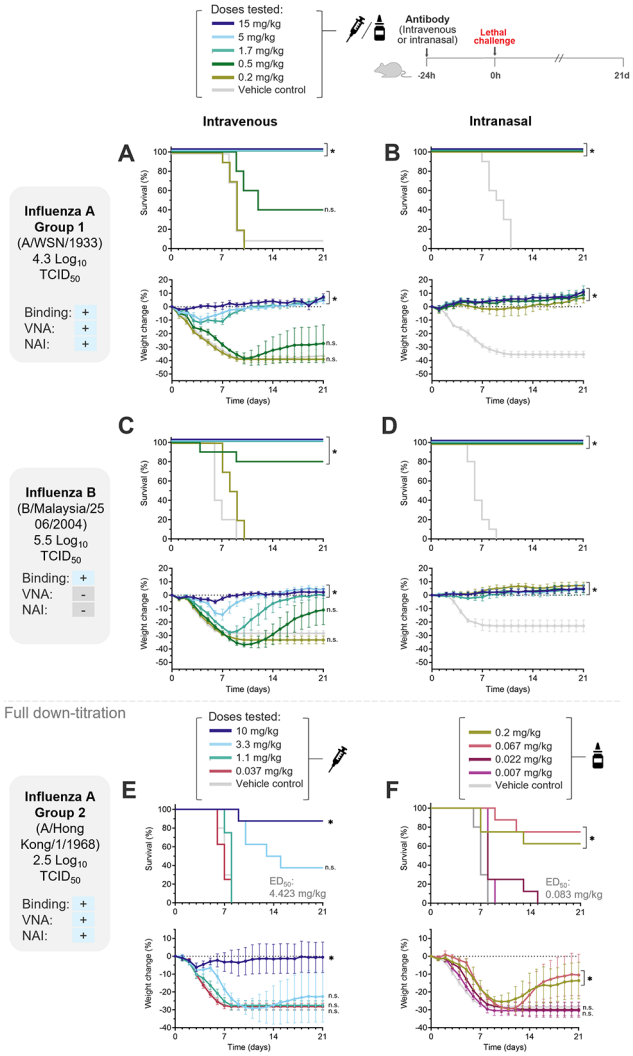

Fig. 2. Intranasal administration of CR9114 at the site of viral entry has dose-sparing effect compared with intravenous administration, for neutralized influenza A/H1N1 and A/H3N2 as well as non-neutralized B/Victoria. Kaplan–Meier survival curves showing in vivo protection by intravenous or intranasal CR9114 in a murine lethal challenge model against influenza A or B viruses. Efficacy of (**A**) intravenous or (**B**) intranasal CR9114 against lethal challenge with A/WSN/1933 (A/H1N1). Efficacy of (**C**) intravenous or (**D**) intranasal CR9114 against lethal challenge with B/Malaysia/2506/2004 (Victoria lineage). Efficacy of (**E**) intravenous or (**F**) intranasal CR9114 against lethal challenge with A/Hong Kong/1/1968 (H3N2). Survival curves (top panels) and change in body weight (bottom panels) of mice treated with indicated doses of CR9114 via intravenous or intranasal administration or PBS control are shown. Grey panels (left) show challenge strain, challenge dosage and indicate whether CR9114 can bind, neutralize ('VNA'), and inhibit NA activity of viruses ('NAI') with yes ('+') or no ('–'). Asterisks indicate significant differences in survival proportions at day 21 and bodyweight change relative to day 0 compared with PBS control ($P < 0.05$). "n.s." indicates not significant compared with PBS control. These experiments were performed with 8–10 mice per group.

mice receiving CR9114 intravenously were fully protected from mortality at 1.7 mg/kg against influenza A/H1N1 virus (Fig. 2A) and at 5 mg/kg against influenza B/Vic virus (Fig. 2C), whereas mice receiving CR9114 via intranasal administration were fully protected at the lowest dose tested of 0.2 mg/kg against both influenza strains (Fig. 2B,D). Following intravenous administration of CR9114, mice suffered weight loss at some dosages that protected from mortality (1.7 mg/kg and 5 mg/kg), whereas no weight loss was observed in mice receiving intranasally-administered CR9114.

For protection against influenza A/H1N1 and influenza B/Vic, we could not precisely quantify the dose reduction, as intranasal CR9114 was still 100% protective at the lowest dosage tested. We therefore also tested protection against A/H3N2, titrating down to lower dosages. Following intravenous administration, CR9114 only provided significant protection against mortality and weight loss at a dose of 10 mg/kg (Fig. 2E). Following intranasal administration, CR9114 provided significant protection against mortality and weight loss at doses as low as 0.2 mg/kg and 0.067 mg/kg (Fig. 2F). The median effective dosage (ED_{50}) was 4.423 mg/kg for intravenous CR9114 and 0.083 mg/kg for intranasal CR9114 (Supplementary Table S6). Thus, intravenously-administered CR9114 was 53-fold less potent than intranasally-administered CR9114 (fold change in median effective dosage: 53.1; 95% CI: 25.1 – 112.3).

We also seized the opportunity to confirm whether the breadth of protection exhibited by CR9114 via the intravenous route, as previously demonstrated in the work of *Dreyfus* et al.[6], is conserved when CR9114 was administered intranasally. To this end, we administered de-escalating doses of CR9114 (15–0.2 mg/kg) intranasally in mice challenged with A/H5N1 (A/Hong Kong/156/1997) or B/Yamagata (B/Florida/4/2006). Intranasal administration of CR9114 potently protected mice from mortality and weight loss (Fig. 3): all tested doses down to 0.2 mg/kg provided significant protection against mortality and weight loss from lethal challenge with H5N1 and B/Yamagata.

Taken together, these data demonstrate that i) direct administration of CR9114 to the respiratory mucosa requires a lower effective dose to ensure a protective effect; ii) intranasally-administered CR9114 protects at low dosage independent of microneutralization read-out (positive for H1N1, H5N1, H3N2; negative for B/Yam and B/Vic) and neuraminidase inhibition (positive for H1N1, H5N1, H3N2, B/Vic; negative for B/Yam).

Intranasal prophylaxis with CR9114 is independent of the Fc domain

The effect of the administration route provided the opportunity to examine the hypothesis that neutralizing activity is operable when the antibody titer is high, whereas Fc-dependent effector functions are essential for protection at low antibody titers. Accordingly, we again performed dose down-titrations of passively-administered antibody through the intravenous and intranasal administration routes 24 hours before challenge. This time, we varied the CR9114 configuration, using wild-type IgG (CR9114-WT), LALA[40] or N297Q[41] mutants (CR9114-LALA, CR9114-N297Q; harboring substitutions that disrupt the binding of the Fc region to Fc receptors on immune cells, thereby reducing or ablating Fc-mediated effector functions) or the bivalent antigen-binding site only ($F(ab')_2$) (Figs. 4 and 5).

For intravenous protection against A/H1N1, the downregulation of Fc effector functions (CR9114-LALA and CR9114-N297Q) and the removal of the Fc tail ($F(ab')_2$) resulted in a marked increase in the median effective dosage (ED_{50}) compared to wild-type (Supplementary Fig. 4 and Table S6). The ED_{50} for CR9114-LALA (1.623 mg/kg) was 7.3-fold higher than CR9114-WT (0.222 mg/kg). This difference was statistically significant (95% CI: 2.32–23.5). The ED_{50} for CR9114-$F(ab')_2$ (71.419 nmol/kg) was 7.9-fold higher than CR9114-N297Q (9.055 nmol/kg; Fig. 6A, Supplementary Fig. 5 and Table S6), also a statistically significant difference (95% CI 3.50–17.8).

On the contrary, when CR9114 was instilled intranasally, low-dosage protection was also observed for all configurations. Neither downregulation of Fc-mediated effector functions nor removal of the Fc tail resulted in statistically significant increases in the ED_{50} (S5 and Table S6), although there was a trend towards slightly higher ED_{50} for the Fc-mutants and $F(ab')_2$ compared to wildtype IgG. The difference in ED_{50} between intranasally-administered CR9114-WT and CR9114-LALA was not statistically significant (1.82-fold; 95% CI 0.56–5.90), nor the difference between CR9114-N297Q and CR9114-$F(ab')_2$ (1.75-fold; 95% CI: 0.66–4.61).

When mice were challenged with B/Yamagata, intravenous administration of CR9114-WT, -LALA, and -N297Q protected from mortality and weight loss only at the highest dosage(s) (Fig. 5). The downregulation of Fc effector functions heavily reduced the protective efficacy of intravenously-administered CR9114. The ED_{50} for CR9114-LALA (5.530 mg/kg) was 29.8-fold higher than CR9114-WT (0.186 mg/kg). The difference was statistically significant (95% CI: 9.2–97.0). Moreover, none of the tested $F(ab')_2$ doses (up to 45 mg/kg; molar equivalent of 68 mg/kg CR9114 IgG) yielded significant protection compared to PBS controls, hence no dosage provided 50% protection and no fold difference between ED_{50}s could be calculated.

In contrast, when CR9114 Fc mutants or $F(ab')_2$ were administered intranasally, mice were protected against mortality and weight loss. Intranasal administration was also marked with a less prominent increase in median effective dosage. The ED_{50} for CR9114-LALA (0.326 mg/kg) was 3.1-fold higher than CR9114-WT (0.104 mg/kg; Fig. 6A). This difference was statistically significant (95% CI: 1.16–8.50). CR9114-N297Q and CR9114-$F(ab')_2$ protected more than 50% of mice from lethal challenge at the lowest dosages tested, so it was not possible to fit a dose–response curve, calculate ED_{50} and determine the fold difference. These data indicate that intranasally-administered antibody is more potent if it contains the Fc domain (Supplementary Figs. 4 and 5), although the relative contribution of Fc is much lower than for intravenously-administered antibody.

We further extended our studies and antibody dosing ranges to evaluate protection against influenza A/H3N2, an influenza group A2 virus that is bound and neutralized by CR9114, albeit less potently compared to A/H1N1 (Fig. 1E; Supplemental Fig. 6). Intravenously-administered full-length CR9114 protected against A/H3N2 at 10 mg/kg, but CR9114-$F(ab')_2$ did not protect even at the highest dosage tested (75 mg/kg; given its lower molecular weight, this is equimolar to a dosage of 113 mg/kg of CR9114 IgG).

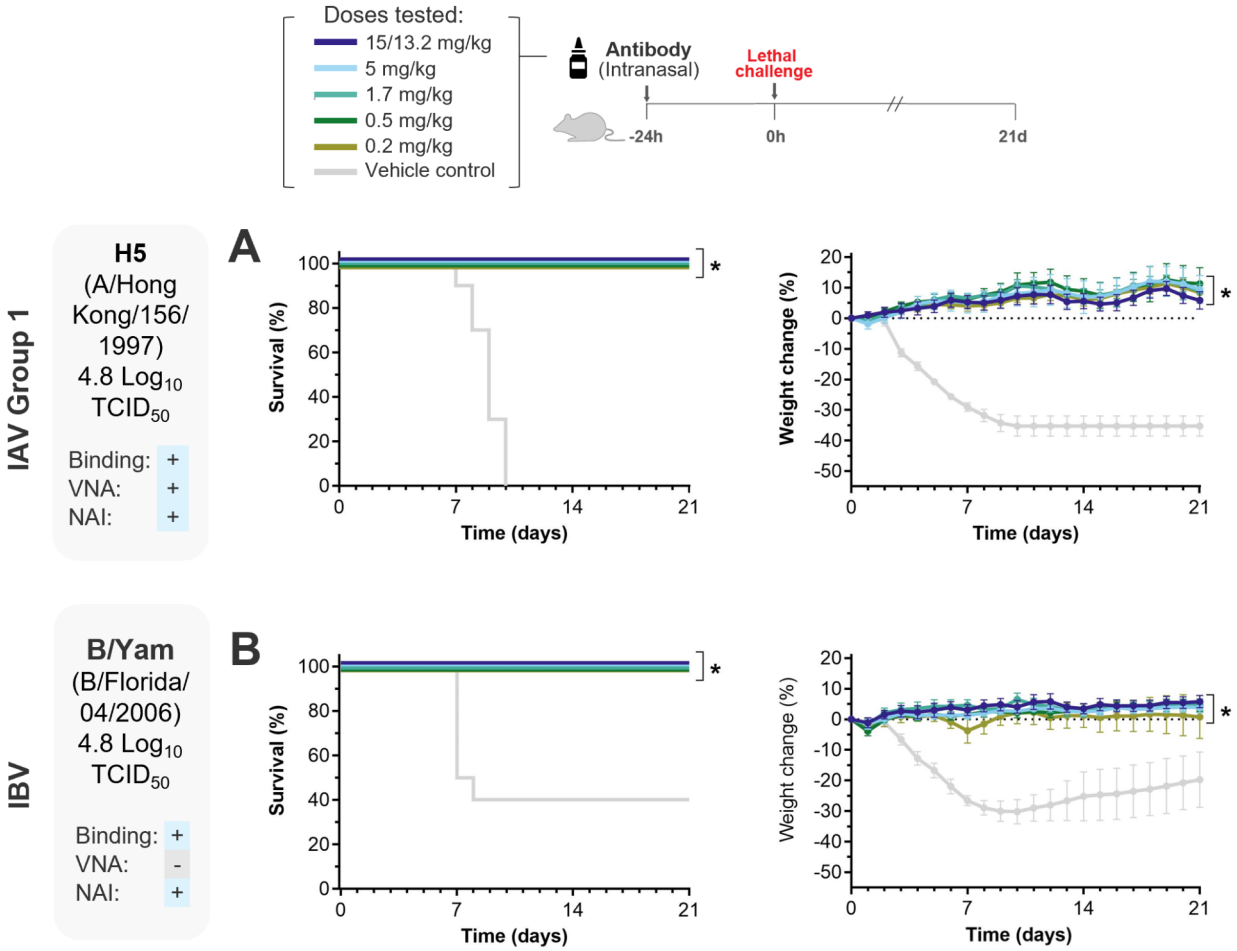

Fig. 3. Intranasal administration of CR9114 potently protects against neutralized avian influenza A/H5N1 and non-neutralized B/Yamagata. Kaplan–Meier survival curves showing the in vivo protection by intranasal CR9114 in a murine lethal challenge model against (**A**) A/Hong Kong/156/1997 (A/H5N1) and (**B**) B/Florida/4/2006 (Yamagata lineage). Survival curves (left panels) and change in body weight (right panels) of mice treated with indicated doses of CR9114 via intranasal administration or PBS control are shown. Grey panels (left) show challenge strain, challenge dosage and indicate whether CR9114 can bind, neutralize ('VNA'), and inhibit NA activity of viruses ('NAI') with yes ('+') or no ('–'). Asterisks indicate significant differences in survival proportions at day 21 and bodyweight change relative to day 0 compared with PBS control ($P < 0.05$). The highest dosage of B/Yamagata challenge differ slightly from that in the H5N1 model. This did not have a scientific reason but was due to a miscalculation in the dilution process (animals in the B/Yamagata challenge model received 13.2 mg/kg—blue line in panel B; animals in the H5N1 challenge model received 15 mg/kg—blue line in panel **A**).

In contrast, when administered intranasally, both full-length CR9114-WT and the CR9114-F(ab′)$_2$ protected against mortality (at 0.2 mg/kg and 1 mg/kg, respectively) and weight loss (at 0.067 mg/kg and 0.11 mg/kg, respectively). When comparing ED$_{50}$s from the dose–response curves, CR9114-WT provided 4.45-fold more potent protection compared to CR9114-F(ab′)$_2$ (95% CI: 2.03–9.72). This data further supports the observation that the Fc-tail is necessary for intravenous protection, but not for intranasal protection, although it does contribute to intranasal potency.

In summary, following challenge with influenza A and B, we recapitulated the impact of administration route as was observed for full-length, wild-type CR9114 (Fig. 2): efficacy of CR9114 was less affected by de-escalating the dose following intranasal administration compared to intravenous administration for all configurations of the antibody. Moreover, we demonstrate that in contrast to intravenous administration, where prophylaxis requires the antibody Fc-tail to protect against both influenza A and B, intranasal protection is Fc-independent. Without its Fc domain, the potency of CR9114 is generally lower than the other full-length IgG configurations, but F(ab′)$_2$ is sufficient to provide local prophylactic protection if administered directly to the site of infection.

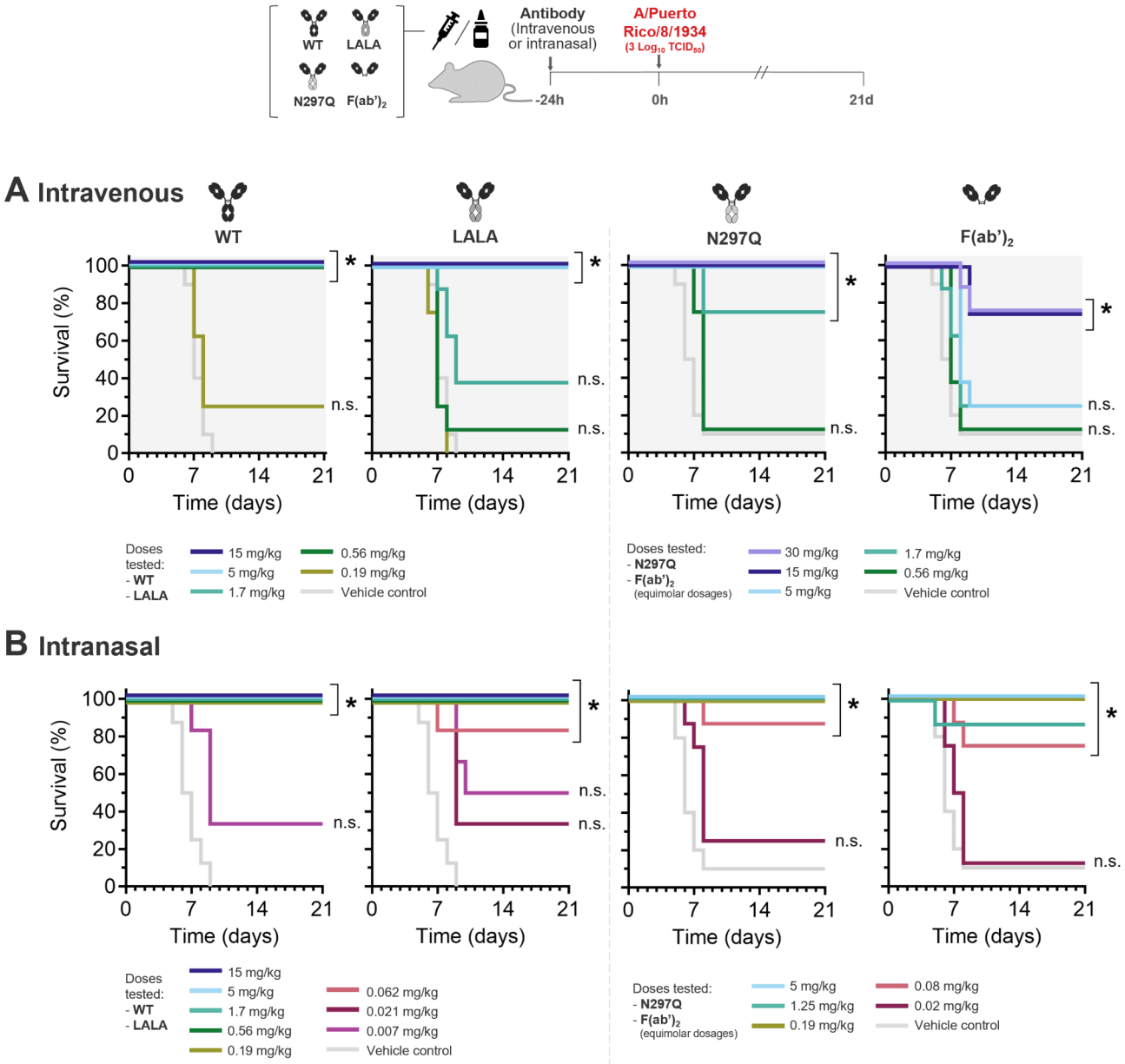

Fig. 4. Intranasal administration route reveals low dose protection against influenza A independent of the antibody Fc, conferred by F(ab')$_2$ alone. (**A**, **B**) Kaplan–Meier survival curves showing the in vivo efficacy of (**A**) intravenous and (**B**) intranasal administration of CR9114, CR9114-LALA, CR9114-N297Q, and CR9114-F(ab′)$_2$ in protecting mice against lethal challenge with influenza A/H1N1 (A/Puerto Rico/8/1934). Mice were treated with indicated doses of CR9114 or PBS via intravenous or intranasal administration 24 h before challenge as shown in the legend. Asterisks indicate significant differences in survival proportions at day 21 compared with PBS control ($P < 0.05$). "n.s." indicates not significant compared with PBS control. Table S4 provides detailed information on the dose titration for each mouse group. Changes in body weight are presented in Fig. S3 and Table S5. These experiments were performed with 8–10 mice per group.

Discussion

We demonstrate that the Fc-dependence or independence of antibody-based immune protection is conditional on the route of antibody administration. Protection conferred by intranasal administration to the site of viral entry and initial infection does not require the Fc domain (Fig. 6). Protection conferred by systemic administration, on the other hand, hinges on the contribution of the Fc domain for both neutralized and non-neutralized strains, and is necessary for non-neutralized strains (Fig. 6).

Furthermore, the dose-sparing effect of intranasal compared to systemic administration suggests that delivering anti-influenza prophylactics to the respiratory mucosa maximizes potency. Systemic administration greatly dilutes antibody concentration at the mucosal site of infection in mice[42,43] and humans[44–46], making Fc effector functions essential for effective protection[8,21,25–27] and sufficient half-life[47].

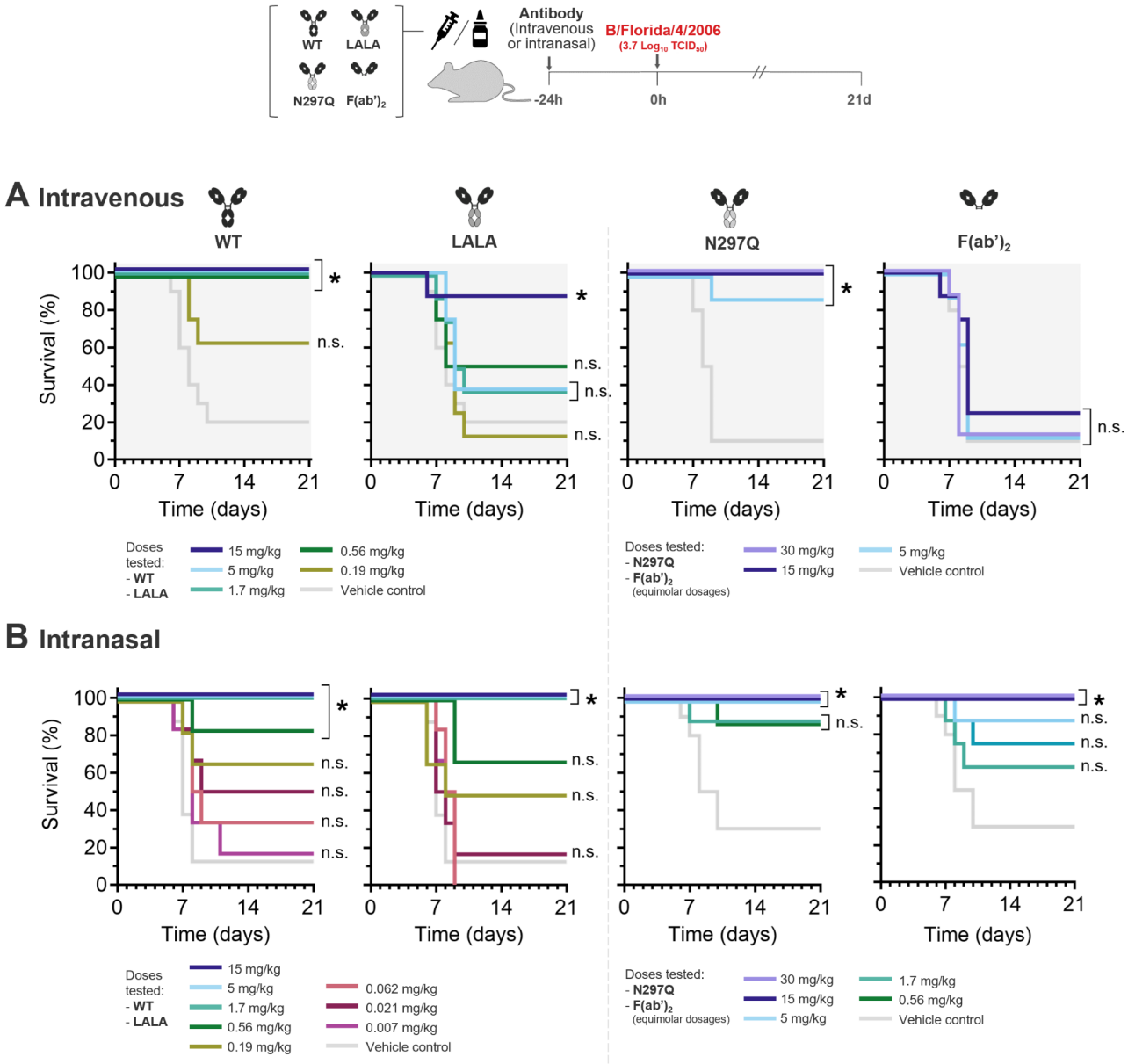

Fig. 5. Intranasal administration of CR9114—unlike intravenous administration—results in protection against influenza B independent of the antibody Fc, conferred by $F(ab')_2$ alone. (**A**, **B**) Kaplan–Meier survival curves showing the in vivo efficacy of (**A**) intravenous and (**B**) intranasal administration of CR9114, CR9114-LALA, CR9114-N297Q, and CR9114-$F(ab')_2$ in protecting mice against lethal challenge with influenza B/Yam (B/Florida/4/2006). Mice were treated with indicated doses of CR9114 or PBS via intravenous or intranasal administration 24 h before challenge as shown in the legend. Asterisks indicate significant differences in survival proportions at day 21 compared with PBS control ($P < 0.05$). "n.s." indicates not significant compared with PBS control. Table S4 provides detailed information on the dose titration for each mouse group. Changes in body weight are presented in Fig. S3 and Table S5. These experiments were performed with 8–10 mice per group.

We have shown that neither Fc effector functions nor in vitro neutralization are necessary for in vivo protection by intranasally-administered CR9114. CR9114–$F(ab')_2$ protects against influenza B when administered intranasally, directly to the respiratory mucosa, but not when administered intravenously. Hence, protection against influenza B by CR9114 IgG is not captured by in vitro microneutralization as a correlate of protection. The lack of neutralization against influenza B virus can be overcome by increasing the avidity of CR9114, consistent with avidity effects reported for viral neutralization by antibodies in other studies[32–35].

For intravenous administration, CR9114 also provides effective protection against neutralized strains in the absence of Fc effector functions (albeit at higher dosages), highlighting the primary role of neutralization under these conditions. This is consistent with a recent study in non-human primates demonstrating that intravenous

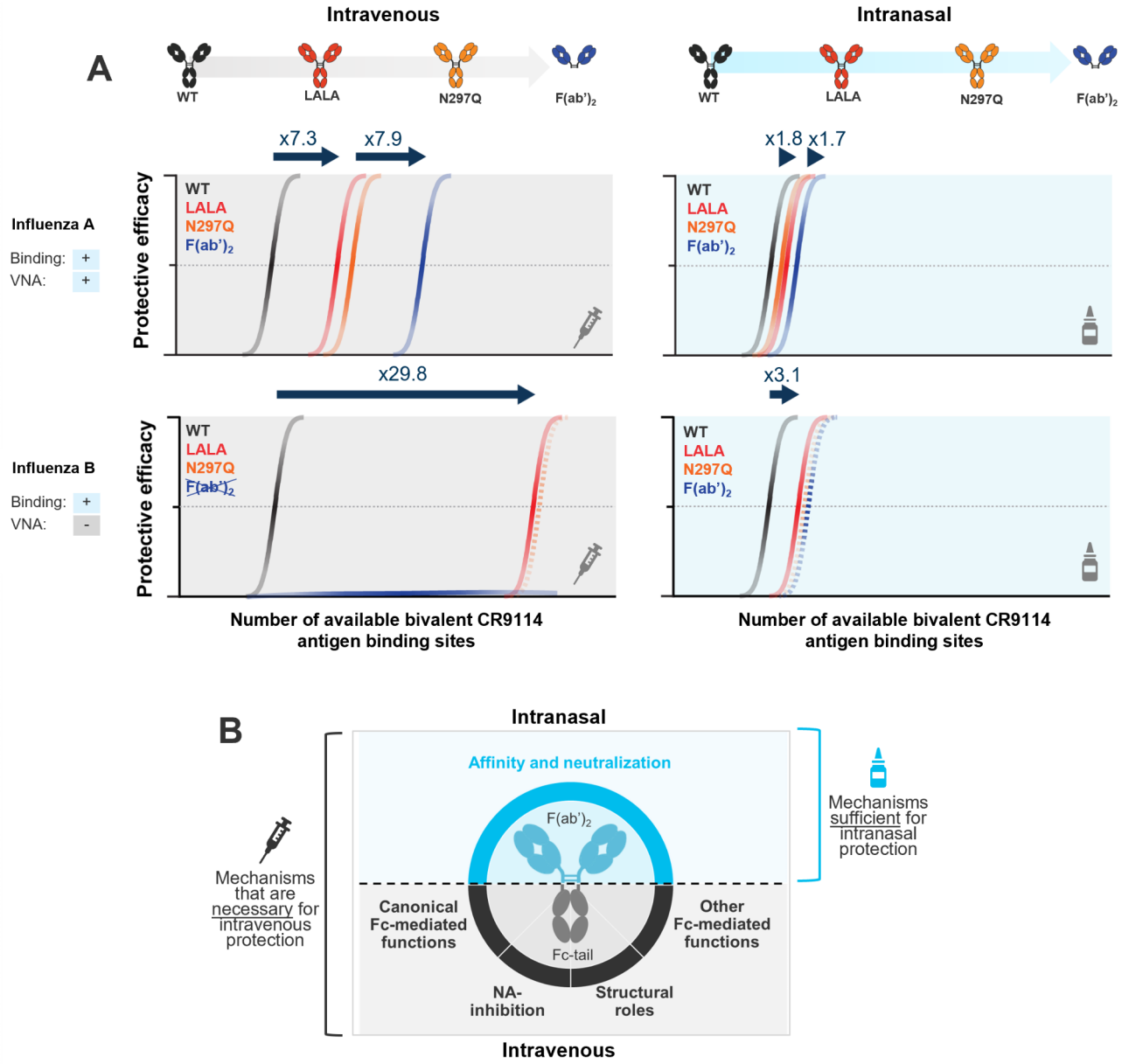

Fig. 6. Administration route reveals Fc-dependent versus independent mechanisms of protection. (**A**) Schematic showing the observed differences in the median effective dose (ED_{50}) of CR9114 IgG, IgG Fc-mutants, or $F(ab')_2$ when administered via the intravenous (left panels) or intranasal route (right panels). (**B**) Schematic showing the necessary and sufficient mechanisms of action mediated by intravenously-(left) or intranasally-administered (right) pan-influenza antibody CR9114.

administration of a neutralizing antibody provides effective protection against sublethal challenge with influenza A/H5N1, even when the antibody harbors mutations that disrupt Fc effector functions[28].

Antibody half-life likely plays a role in the lower efficacy of intravenously-administered $F(ab')_2$, given that it has a lower serum half-life in mice compared to IgG[47]. Even if equimolar dosages are administered at the start of the study, serum concentrations of IgG/LALA/N297Q versus $F(ab')_2$ may differ at the time of challenge. When administered intratracheally, half-life of IgG and $F(ab')_2$ in the respiratory tract are comparable[47], but to date, no studies on half-life following intranasal administration in a murine model have been published[42].

We used Fc-knockdown and knockout formats in BALB/c mice and 129X1/SvJ mice to test Fc-dependence, rather than Fc-knockout mice. Our results on intravenously-administered CR9114 are consistent with a study of Fc-dependence testing CR9114-wildtype in Fc-knockout mice against neutralized versus non-neutralized H2N2 strains[8]. This study also found that intravenously-administered CR9114 requires Fc effector functions for protection against non-neutralized strains.

It was previously reported that intranasal CR9114 does not protect against influenza B virus in a post-exposure setting[48]. Therapeutic applications of intranasal CR9114 may therefore be different or require alternative approaches. Once the virus has spread to the systemic compartment, systemic antibody penetration and Fc effector functions may confer more benefits than in the pre-exposure setting[41].

Collectively, our observations reveal in vivo antiviral activity by the bivalent antigen binding site that is neither reliant on the antibody Fc, nor captured by standard microneutralization measurements in vitro. One should not generalize this finding to influenza prophylaxis in general until Fc-independence of the intranasal administration route has been investigated for an additional antibody, for example against the hemagglutinin receptor-binding domain or against neuraminidase.

We conclude that the local molarity of the antibody at the relevant site of infection will not only determine the strength of humoral immunity but will also dictate the dominant mode (Fc-dependent versus Fc-independent) of antibody protection. We anticipate that these results will inform the design of clinical strategies for pre-exposure protection to achieve maximal prophylactic potency, including in populations where immune response after influenza vaccination is suboptimal, like the elderly and immunocompromised.

Materials and methods

Study design

This study was designed to determine the protective activity of influenza mAb CR9114 following intranasal and intravenous administration in murine challenge models. The study aimed to define route-specific mechanisms of broad protection, namely, how the role of CR9114 $F(ab')_2$ and the Fc-tail differ across the administration route and influenza virus. Comparisons were made by administering wild-type (WT), Fc-variants, or $F(ab')_2$ of CR9114 via the intravenous or intranasal route prior to virus challenge with influenza A or B. In each case, we compared the dose-dependent response of CR9114 against morbidity and mortality in mice. Mice were assigned to groups using a computerized randomization procedure.

Group sizes were determined on the basis of a 2-sided Fisher's exact test with at least 80% power to detect an absolute difference of 60–80% in survival between a treatment and control group at the two-sided 5% significance level. In case multiple comparisons were planned, the significance level was adjusted according to Bonferroni.

Details on study numbers and inclusion/exclusion criteria for statistical analysis are described under "In vivo efficacy of CR9114 against influenza". Studies have been reported according to ARRIVE (Animal Research: Reporting of In Vivo Experiments) guidelines for animal research.

In silico modeling

The three-dimensional (3D) structures of the H5-CR9114 (PDB ID: 4FQI), H3-CR9114 (PDB ID: 4FQY), and B/Victoria-CR9114 (PDB ID: 6CNV) complex were obtained the Protein Data Bank. The H1-CR911 complex was built by using PDB ID: 5VLI (Computationally designed inhibitor peptide HB1.6928.2.3 in complex with influenza hemagglutinin (A/Puerto Rico/8/1934) and PDB ID: 5CJQ (Crystal structure of a trimeric influenza hemagglutinin stem in complex with a broadly neutralizing antibody CR9114). The B/Yamagata-CR9114 complex was modeled based on the PDB ID: 6CNV and PDB ID 4M40 (Crystal structure of hemagglutinin of influenza virus B/Yamanashi/166/1998). The 3D structures of the Hemagglutinin-Esterase-Fusion (HEF) protein of influenza C (PDB ID: 1FLC) and D (PDB ID: 5E64) were also retrieved from the PDB. The complexes between CR9114 and HEF-Influenza C/HEF-Influenza D were generated using the HADDOCK 2.2 webserver[49].

All these complexes were subjected to molecular dynamics (MD) simulations and binding free energy (BFE) calculations by applying standard parameters and protocols as previously described[50,51]. Briefly, the Amber ff19SB force field was assigned for influenza proteins (HA and HEFs) and CR9114, and the OPC water model was used. The time step of MD simulations was set to 2 fs by applying SHAKE constraint. The temperature and pressure of the systems were fixed to 300 K and 1 bar, respectively. The MD simulations were performed for 500 ns and the snapshots from the last 50 ns of MD simulations (450–500 ns, 100 snapshots) were extracted for BFE calculations by using molecular mechanics/generalized Born surface area (MM/GBSA) method (igb = 8 model). MD simulations and BFE calculations were executed by the utilization of the AMBER 22 program[52].

Antibodies

Human IgG1 antibodies, CR9114, CR9114-LALA, CR9114-N297Q, and CR9114-$F(ab')_2$ were expressed and purified as recombinant mAb in HEK293-253 cells. The heavy and light chain variable regions were cloned into a single expression vector, which was used to transfect HEK293-253 cells. Six days post-transfection, the expressed antibodies were purified from the medium using MabSelect PrismA chromatography. Protein-containing fractions were pooled and concentrated before an additional purification step by gel filtration using a Superdex200 Increase26/40 column. Protein-containing fragments were analyzed by LapChip® capillary electrophoresis and antibody-containing fractions were pooled.

Two other batches of CR9114-IgG1 were also produced in PerC6 cells (used for the in vivo studies shown in Figs. 2 and 3).

Live virus microneutralization assays

Twofold serial dilutions of CR9114 (highest final concentration of 100 ug/mL) or Ribavirin (500 ug/mL) were mixed with 500 PFUs of the following viral strains in a 96-well plate: A/Michigan/45/2015 (H1N1), A/HongKong/01/1968 (H3N2), B/Brisbane/60/2008 (B Victoria lineage), and B/Florida/04/2006 (B Yamagata lineage). The mixtures were incubated with MDCK cells for 90 min at 35 °C and 5% CO_2, and then washed with medium containing CR9114/Ribavirin at the same dilution but with no virus. The places were then incubated for ~ 24 h (for H1N1 and H3N2) or ~ 48 h (B Victoria and Yamagata lineage) at 35 °C and 5% CO_2. To control for the quantity of virus input, working dilutions of the virus were also back-titrated onto cells in the absence

of CR9114/Ribavirin. These cells were first incubated for 90 min, and then medium containing carboxymethyl cellulose (CMC) to confine viral progeny to the site of infection was added to facilitate the microplaque count; the cells were then incubated for ~ 48 h in the presence of CMC. After completion of the incubation period of CR9114/Ribavirin-treated cells and the back titrated cells, the cells were formalin-fixed (in the presence of Triton X-100), and immunolabelled with an anti-influenza A or B nucleoprotein primary antibody and anti-horse radish peroxidase secondary antibody. TrueBlue™ peroxidase substrate was used for visualization of the virus-positive cells using a CTL Immunospot analyzer. The percentage of virus-positive cells (virus signal) was used to calculate the IC_{50} as described in[53].

Pseudotyped virus microneutralization assays

The pseudotype neutralization assay was performed following the protocol by *Ferrara* et al.[54] with the following Influenza strains: C/Minnesota/33/2015, D/Bovine/Italy/46484/2015, and D/Bovine/France/5920/2014. Antibody concentrations ranging from 0.49 to 1000 ng/mL were used. Briefly, 50 µL of PV at a titer of 1.0×10^6 RLU/well, as determined by titration, was added to the mAb. The mixture was then incubated for 1 h at 37 °C with 5% CO2. Afterwards, 50 µL of HEK293T/17 cells at a concentration of 1.5×10^4 cells/well were added to each well. PV-only controls (representing 0% neutralization) and cell-only controls with no virus (representing 100% neutralization) were also included on the test plate. Plates were then incubated for 48 h at 37 °C and 5% CO_2. Media was removed and 25 µL of the Bright-Glo® luciferase assay substrate added to each well. Plates were read using the GloMax® Navigator (Promega, Southampton, UK) using the Promega GloMax® Luminescence Quick-Read protocol.

Relative Light Unit (RLU) values were normalized against the PV-only and cell-only controls, which represent 0% and 100% neutralization responses, respectively. The resulting neutralization-antibody dose–response curve was modeled using a 4-parameter logistic curve with fixed plateaus at 0% and 100%, incorporating a sample-specific slope and IC_{50}. The IC_{50} values presented in Fig. 1E are the geometric mean of the IC_{50} values calculated from two technical replicates.

Enzyme-linked lectin assay (ELLA)

To measure the NA inhibitory activity of CR9114 using an immobilized substrate, the ELLA assay was performed. To determine the amount of virus to use in the ELLA assay, each virus (H1 A/Puerto Rico/8/1934, H3 A/Cambodia/e0826360/2020, B/Malaysia/2506/2004, and B/Phuket/3073/2013) was serially diluted twofold and added to fetuin-coated plates for a 16–18 h incubation period at 37 °C and 5% CO_2. Plates were then washed and incubated with *Arachis hypogaea* Lectin-Horseradish Peroxidase for 1 h. Next, the plates were washed again, and incubated for 15 min with o-Phenylenediamine dihydrochloride as a substrate. Absorbance was detected at 490 nm using the Spectramax Paradigm plate reader. The working virus dilution for each virus Lot was determined as the dilution that corresponds to 90% NA activity. To assess NA inhibition by CR9114, the same protocol was followed but with the addition of CR9114 (starting concentration: 64 µg/mL). CR9114 was serially diluted threefold and added to an equal volume of the virus. The mixture was then added to fetuin-coated plates and processed as described above. All samples were assayed in technical triplicate. Raw OD values were imported into GraphPad Prism, and data were analyzed using 4-parameter logistic curve analysis to calculate the IC_{50} value for each sample.

HEF proteins and biolayer interferometry (BLI)

The recombinant HA or HEF ectodomains from influenza A virus (A/Puerto Rico/8/1934 and A/Hong Kong/1968), influenza B virus (B/Florida/4/2006 and B/Brisbane/60/2008), influenza C virus (C/Johannesburg/1/1966)[55] and influenza D virus (D/swine/Oklahoma/1334/2011)[56], were affinity purified following expression in 293F cells according to established methodology[10,11,57–59]. The proteins were expressed using pVRC8400, a plasmid containing the CMV IE Enhancer/Promoter, HTLV-1 R Region and Splice Donor site, and the CMV IE Splice Acceptor site upstream of the open reading frame[60]. In each case, the fold on Avi-His tag was attached to the C-terminus of the ectodomain[10,11,57–59]. The 293F cells were with grown in Freestyle media (Life Technologies) were transfected with 500 µg/L of expression plasmid + pBirAFlag [CMV expression for secreted form of BirA (the enzyme catalyzing biotinylation at the Avi tag sequence); Plasmid # 64395, Addgene] using 293fectin™ Reagent (Life Technologies). After 5 days, the culture was centrifuged (2,000 × *g*, 10 min) and the supernatant was filtered (VacuCap 8/0.2 µm filters, Pall Corporation) and loaded on Ni Sepharose FF resin (GE Healthcare) by gravity flow. The resin was washed (6 column volumes of PBS containing 20 mM imidazole) and the biotinylated-HEF were eluted in 500 mM imidazole. The eluate was separated by size exclusion FPLC (Superdex 200 10/300 column; GE Healthcare) and buffer exchanged into 1xPBS. After concentration of the HEF fraction (Amicon Ultra concentrators, 30 kDa, cut off), the biotinylated-HEFs were immediately deployed for bilayer interferometry (BLI).

BLI was performed using the Personal Assay BLItz System (Fortebio)[10,11,61]. Biotinylated HEF were immobilized onto streptavidin biosensors (Sartorius, Cat#18-5019). After establishing a baseline in kinetic buffer (PBS containing 0.02% Tween20, 0.1% BSA), CR9114 (Fab or IgG or IgM) was applied at 0.625 µM, 1.25 µM, 2.5 µM, and 5 µM, with 60 s of association and 60 s of dissociation. The equilibrium dissociation constant (K_D) values were calculated by fitting a 1:1 binding isotherm using software provided by the vendor. Our instrument cannot resolve K_D values > 100 µM[10,11,61].

In vivo efficacy of CR9114 against influenza

Female BALB/c and 129X1/SvJ specified pathogen-free mice were purchased from Charles River Laboratories and Jackson Laboratories, respectively. Except for the H3N2 challenge study, which used 129X1/SvJ mice, all experiments were performed with the BALB/c mice. In experiments with CR9114, treatment and vehicle control

groups consisted of 10 animals each. In experiments with CR9114-LALA or CR9114-F(ab′)$_2$, treatment and vehicle control groups consisted of 8 and 10 animals each, respectively. Mice were removed from statistical analysis if study deviations occurred resulting in 8–10 animals per group in some challenge studies. Criteria for exclusion from the statistical analysis included: incorrect dosing, death on study day −1 and day 0. Animals were anaesthetized by either inhalation with isoflurane or ketamine (87.5 mg/kg) and xylazine (11 mg/kg) cocktail mixture via the intraperitoneal route.

MAbs were administered by intranasal instillation (15 µL or 50 µL per nostril) or by intravenous injection (5 mL/kg, tail vein) volume of solution containing a total amount of the indicated protein per dose 24 h before inoculation. For dose calculation purposes, an average weight of 20 g was assumed. Antibody treatment or PBS control groups consisted of 8 or 10 mice each, unless specified otherwise. The dosing of antibodies was calculated such that mice received equimolar doses of CR9114, CR9114-LALA, CR9114-N297Q, or CR9114-F(ab′)$_2$.

The anesthetized mice were held such that the nose pointed upwards, and the inoculum (15 µL or 25 µL per nostril) was administered dropwise into the nose. The mouse was held upright to allow the virus to be inhaled thoroughly and then returned to its cage. A full list of viruses used for the challenge and the corresponding $TCID_{50}$ information can be found in Table S3. Clinical signs and body weights were determined daily from one day before the viral challenge (− 1 days) until the end of the study on day 21. Any animals meeting predetermined humane endpoint criteria, as well as all animals surviving to the end of the study were humanely euthanized by CO_2 asphyxiation or cervical dislocation.

Survival proportions at day 21 and change in body weight were compared to the PBS control group using a Fisher's exact test and a Welch's t-test, respectively. For change in body weight, repeated measurements in the challenge phase were summarized as a single outcome per animal using an Area Under the Curve (AUC) approach where missing values for animals that died before day 21 were imputed with a last-observation-carried-forward method. Bodyweight data are expressed as the change relative to the day 0 measurement. The AUC was then defined as the summation of the area above and below the baseline.

When multiple treatments were compared to the control group, a Bonferroni adjustment for multiple comparisons was applied. Within each treatment, dose-wise comparisons to the control group were performed using a stepwise approach, starting with the highest antibody dose and conditionally testing a lower dose if the previous dose was statistically significant. All analyses were performed using *R*, all statistical tests were performed two-sided and P values of < 0.05 were considered significant. Where applicable, in the Kaplan–Meier survival curves, lines were nudged relative to the *y*-axis to improve visual representation.

ED_{50}'s were estimated from survival dose–response curves using Probit regression. In case of survival in the vehicle control group, survival proportions were adjusted for the natural response rate using Abbott's method[62]; and to adjust for differences in molecular weights, doses (in mg/kg) were converted to nmol/kg.

All animal procedures were performed in accordance with the protocols and reviewed and approved by the Dutch Central Authority for Scientific Procedures on Animals. In IITRI's animal biosafety level–2 suite, all animal procedures were performed in accordance with the protocols approved by the animal care and use committee at IIT Research Institute (IACUC protocol #22-013).

Data preparation

Graphs generated in GraphPad Prism and, where necessary, imported into Adobe Illustrator for aesthetical adjustment.

Data availability

The following protein structures are freely available from the Protein Data Bank: H5 HA – CR9114 complex (PDB ID: 4FQI), H3 HA – CR9114 (PDB ID: 4FQY), B/Victoria HA – CR9114 complex (PDB ID: 6CNV), H1 HA (PDB ID: 5VLI and PDB ID: 5CJQ) B/Yamagata HA (PDB ID: 6CNV and PDB ID: 4M40), influenza C HEF (PDB ID: 1FLC) and influenza D HEF (PDB ID: 5E64). Nucleotide sequences for CR9114 variable regions have been deposited in GenBank (accession numbers JX213639 and JX213640 for VH and Vλ, respectively). Correspondence and requests for materials should be addressed to A.L.B.

Received: 26 August 2024; Accepted: 12 March 2025
Published online: 08 April 2025

References

1. World Health Organization. Influenza (Seasonal)—Fact sheet. https://www.who.int/news-room/fact-sheets/detail/influenza-(seasonal) (2023).
2. World Health Organization. Influenza (Avian and other zoonotic)—Fact sheet. https://www.who.int/news-room/fact-sheets/detail/influenza-(avian-and-other-zoonotic) (2023).
3. Momont, C. et al. A pan-influenza antibody inhibiting neuraminidase via receptor mimicry. *Nature* https://doi.org/10.1038/s41586-023-06136-y (2023).
4. Sangesland, M. & Lingwood, D. Antibody focusing to conserved sites of vulnerability: The immunological pathways for 'universal' influenza vaccines. *Vaccines (Basel)* **9**, 125 (2021).
5. Caradonna, T. M. & Schmidt, A. G. Protein engineering strategies for rational immunogen design. *NPJ Vaccines* **6**, 154 (2021).
6. Dreyfus, C. et al. Highly conserved protective epitopes on influenza B viruses. *Science* **1979**(337), 1343–1348 (2012).
7. Beukenhorst, A. L. et al. A pan-influenza monoclonal antibody neutralizes H5 strains and prophylactically protects through intranasal administration. *Sci. Rep.* **14**, 3818 (2024).
8. Sutton, T. C. et al. In vitro neutralization is not predictive of prophylactic efficacy of broadly neutralizing monoclonal antibodies CR6261 and CR9114 against lethal H2 influenza virus challenge in mice. *J. Virol.* **91**, 10–1128 (2017).
9. Sangesland, M. et al. Germline-encoded affinity for cognate antigen enables vaccine amplification of a human broadly neutralizing response against influenza virus. *Immunity* **51**, 735-749.e8 (2019).

10. Sangesland, M. et al. Allelic polymorphism controls autoreactivity and vaccine elicitation of human broadly neutralizing antibodies against influenza virus. *Immunity* **55**, 1693-1709.e8 (2022).
11. Ray, R. et al. Eliciting a single amino acid change by vaccination generates antibody protection against group 1 and group 2 influenza A viruses. *Immunity* **57**, 1141-1159.e11 (2024).
12. Ekiert, D. C. et al. A highly conserved neutralizing epitope on group 2 influenza A viruses. *Science* **1979**(333), 843–850 (2011).
13. Pantaleo, G., Correia, B., Fenwick, C., Joo, V. S. & Perez, L. Antibodies to combat viral infections: Development strategies and progress. *Nat. Rev. Drug Discov.* **21**, 676–696 (2022).
14. Bournazos, S. & Ravetch, J. V. Fcγ receptor function and the design of vaccination strategies. *Immunity* **47**, 224–233 (2017).
15. Boudreau, C. M. & Alter, G. Extra-neutralizing FcR-mediated antibody functions for a universal influenza vaccine. *Front. Immunol.* **10**, 440 (2019).
16. Nimmerjahn, F. & Ravetch, J. V. Fcγ receptors as regulators of immune responses. *Nat. Rev. Immunol.* **8**, 34–47 (2008).
17. Bournazos, S. & Ravetch, J. V. Diversification of IgG effector functions. *Int. Immunol.* **29**, 303–310 (2017).
18. Rudraraju, R. & Subbarao, K. Passive immunization with influenza haemagglutinin specific monoclonal antibodies. *Hum. Vaccin. Immunother.* **14**, 1–9. https://doi.org/10.1080/21645515.2018.1489947 (2018).
19. Cho, A. & Wrammert, J. Implications of broadly neutralizing antibodies in the development of a universal influenza vaccine. *Curr. Opin. Virol.* **17**, 110–115. https://doi.org/10.1016/j.coviro.2016.03.002 (2016).
20. Vanderven, H. A., Jegaskanda, S., Wheatley, A. K. & Kent, S. J. Antibody-dependent cellular cytotoxicity and influenza virus. *Curr. Opin. Virol.* **22**, 89–96 (2017).
21. Dilillo, D. J., Tan, G. S., Palese, P. & Ravetch, J. V. Broadly neutralizing hemagglutinin stalk-specific antibodies require FcR interactions for protection against influenza virus in vivo. *Nat. Med.* **20**, 143–151 (2014).
22. Vigil, A., Frias-Staheli, N., Carabeo, T. & Wittekind, M. Airway delivery of anti-influenza monoclonal antibodies results in enhanced antiviral activities and enables broad-coverage combination therapies. *J. Virol.* **94**, 10–1128 (2020).
23. Beukenhorst, A. L. et al. The influenza hemagglutinin stem antibody CR9114: Evidence for a narrow evolutionary path towards universal protection. *Front. Virol.* **2**, 1049134 (2022).
24. Nachbagauer, R. et al. A chimeric hemagglutinin-based universal influenza virus vaccine approach induces broad and long-lasting immunity in a randomized, placebo-controlled phase I trial. *Nat. Med.* **27**, 106–114 (2021).
25. He, W. et al. Epitope specificity plays a critical role in regulating antibody-dependent cell-mediated cytotoxicity against influenza A virus. *Proc. Natl. Acad. Sci.* **113**, 11931–11936 (2016).
26. Corti, D. et al. A neutralizing antibody selected from plasma cells that binds to group 1 and group 2 influenza A hemagglutinins. *Science* **1979**(333), 850–856 (2011).
27. Boudreau, C. M. et al. Antibody-mediated NK cell activation as a correlate of immunity against influenza infection. *Nat. Commun.* **14**, 5170 (2023).
28. Kanekiyo, M. et al. Pre-exposure antibody prophylaxis protects macaques from severe influenza. *Science* **1979**(387), 534–541 (2025).
29. Liu, R., Sheng, Z., Huang, C., Wang, D. & Li, F. Influenza D virus. *Curr. Opin. Virol.* **44**, 154–161 (2020).
30. Wang, M. & Veit, M. Hemagglutinin-esterase-fusion (HEF) protein of influenza C virus. *Protein Cell* **7**, 28–45 (2016).
31. Halldorsson, S., Sader, K., Turner, J., Calder, L. J. & Rosenthal, P. B. In situ structure and organization of the influenza C virus surface glycoprotein. *Nat. Commun.* **12**, 1694 (2021).
32. Saito, S. et al. IgA tetramerization improves target breadth but not peak potency of functionality of anti-influenza virus broadly neutralizing antibody. *PLoS Pathog.* **15**, e1007427 (2019).
33. Suzuki, T. et al. Relationship of the quaternary structure of human secretory IgA to neutralization of influenza virus. *Proc. Natl. Acad. Sci.* **112**, 7809–7814 (2015).
34. Terauchi, Y. et al. IgA polymerization contributes to efficient virus neutralization on human upper respiratory mucosa after intranasal inactivated influenza vaccine administration. *Hum. Vaccin. Immunother.* **14**, 1351–1361 (2018).
35. Wang, Z. et al. Enhanced SARS-CoV-2 neutralization by dimeric IgA. *Sci. Transl. Med.* **13**, 1555 (2021).
36. Stadlbauer, D. et al. Broadly protective human antibodies that target the active site of influenza virus neuraminidase. *Science* **1979**(366), 499–504 (2019).
37. Chen, Y.-Q., Lan, L.Y.-L., Huang, M., Henry, C. & Wilson, P. C. Hemagglutinin stalk-reactive antibodies interfere with influenza virus neuraminidase activity by steric hindrance. *J. Virol.* **93**, 10–1128 (2019).
38. Rajendran, M. et al. Analysis of anti-influenza virus neuraminidase antibodies in children, adults, and the elderly by ELISA and enzyme inhibition: Evidence for original antigenic sin. *mBio* **8**, 10–1128 (2017).
39. da Costa, K. A. S. et al. Influenza A (N1–N9) and Influenza B (B/Victoria and B/Yamagata) neuraminidase pseudotypes as tools for pandemic preparedness and improved influenza vaccine design. *Vaccines (Basel)* **10**, 1520 (2022).
40. Lund, J. et al. Human Fc gamma RI and Fc gamma RII interact with distinct but overlapping sites on human IgG. *J. Immunol.* **147**, 2657–2662 (1991).
41. Bolt, S. et al. The generation of a humanized, non-mitogenic CD3 monoclonal antibody which retains in vitro immunosuppressive properties. *Eur. J. Immunol.* **23**, 403–411 (1993).
42. Leyva-Grado, V. H., Tan, G. S., Leon, P. E., Yondola, M. & Palese, P. Direct administration in the respiratory tract improves efficacy of broadly neutralizing anti-influenza virus monoclonal antibodies. *Antimicrob. Agents Chemother.* **59**, 4162–4172 (2015).
43. Li, Z. et al. Influence of molecular size on tissue distribution of antibody fragments. *MAbs* **8**, 113–119 (2016).
44. Han, A. et al. Safety and efficacy of CR6261 in an influenza A H1N1 healthy human challenge model. *Clin. Infect. Dis.* **73**, e4260–e4268 (2021).
45. Hershberger, E. et al. Safety and efficacy of monoclonal antibody VIS410 in adults with uncomplicated influenza A infection: Results from a randomized, double-blind, phase-2, placebo-controlled study. *EBioMedicine* **40**, 574–582 (2019).
46. McBride, J. M. et al. Phase 2 randomized trial of the safety and efficacy of MHAA4549A, a broadly neutralizing monoclonal antibody, in a human Influenza A virus challenge model. *Antimicrob. Agents Chemother.* **61**, 10–1128 (2017).
47. Jagdale, P., Verma, A. & Shah, D. K. Pulmonary pharmacokinetics of antibody and antibody fragments following systemic and local administration in mice. *Pharmaceutics* **16**, 1259 (2024).
48. Vigil, A. et al. Native human monoclonal antibodies with potent cross-lineage neutralization of influenza B viruses. *Antimicrob. Agents Chemother.* **62**, 10–1128 (2018).
49. van Zundert, G. C. P. et al. The HADDOCK2.2 web server: User-friendly integrative modeling of biomolecular complexes. *J. Mol. Biol.* **428**, 720–725 (2016).
50. Wichapong, K. et al. Structure-based design of peptidic inhibitors of the interaction between CC chemokine ligand 5 (CCL5) and human neutrophil peptides 1 (HNP1). *J. Med. Chem.* **59**, 4289–4301 (2016).
51. Wichapong, K. et al. Structure-based peptide design targeting intrinsically disordered proteins: Novel histone H4 and H2A peptidic inhibitors. *Comput. Struct. Biotechnol. J.* **19**, 934–948 (2021).
52. Case, D. A. et al. AmberTools. *J. Chem. Inf. Model.* **63**, 6183–6191 (2023).
53. Zielinska, E. et al. Development of an improved microneutralization assay for respiratory syncytial virus by automated plaque counting using imaging analysis. *Virol. J.* **2**, 84 (2005).
54. Ferrara, F. & Temperton, N. Pseudotype neutralization assays: From laboratory bench to data analysis. *Methods Protoc.* **1**, 8 (2018).
55. Rosenthal, P. B. et al. Structure of the haemagglutinin-esterase-fusion glycoprotein of influenza C virus. *Nature* **396**, 92–96 (1998).

56. Song, H. et al. An open receptor-binding cavity of hemagglutinin-esterase-fusion glycoprotein from newly-identified Influenza D virus: Basis for its broad cell tropism. *PLoS Pathog.* **12**, e1005411 (2016).
57. Corbett, K. S. et al. Design of nanoparticulate group 2 influenza virus hemagglutinin stem antigens that activate unmutated ancestor B cell receptors of broadly neutralizing antibody lineages. *mBio* **10**, 497123 (2019).
58. Weaver, G. C. et al. In vitro reconstitution of B cell receptor–antigen interactions to evaluate potential vaccine candidates. *Nat. Protoc.* **11**, 193–213 (2016).
59. Kanekiyo, M. et al. Self-assembling influenza nanoparticle vaccines elicit broadly neutralizing H1N1 antibodies. *Nature* **499**, 102–106 (2013).
60. Wu, X. et al. Rational design of envelope identifies broadly neutralizing human monoclonal antibodies to HIV-1. *Science* **1979**(329), 856–861 (2010).
61. Ronsard, L. et al. Engaging an HIV vaccine target through the acquisition of low B cell affinity. *Nat. Commun.* **14**, 5249 (2023).
62. Abbott, W. S. A method of computing the effectiveness of an insecticide. *J. Econ. Entomol.* **18**, 265–267 (1925).

Acknowledgements

The authors thank the following individuals for their expertise and assistance throughout the study: Wouter Koudstaal, Just Brakenhoff, Ilse Haisma, Salo Ooft, Dennis de Vlaam, Sagrario Arias Rivas, Javante Ishmael-Langham, Allison Bhattacharya, Abigail Bachyrycz, Erwin Claassens, and personnel from WBVR and IITRI. Antibody and virus icons were created in Biorender. Science, R., (2025) https://BioRender.com/n21q845.

Author contributions

A.L.B., K.L.R., J.F., M.H.K., C.M.K., and J.G. contributed to the study conception, with the intellectual input from B.J. and J.C. A.L.B, K.L.R., J.F. and D.L. wrote the first draft of the manuscript. All authors reviewed and approved the manuscript. N.T., and K.A.S.dC planned the pseudotype neutralization experiments. N.T. and K.A.S.dC. carried out pseudotype neutralization experiments. B.A.d.J, H.V, S.F. and M.H.K. designed and planned, and L.A.H.M. oversaw execution of the in vivo experiments corresponding to Fig. 2 and Fig. 3. A.L.B., M.H.K., C.M.K., S.F. designed and planned the in vivo experiments corresponding to Fig. 4 and Fig. 5. M.H.K., J.M.K. carried out statistical analyses. K.W. conducted protein structural analysis using in silico modeling. D.L., L.A., C.M., F.A.N.M., V.O., and L.R. performed the purification of viral spike proteins and corresponding biolayer interferometry. K.L.R. and J.F. performed the data visualization with input from A.L.B., M.H.K and J.M.K.

Funding

This study was financially supported by Leyden Laboratories B.V.

Competing interests

A.L.B., K.L.R., J.F., M.H.K, C.M.B., J.C., B.A.d.J., S.F., J.M.K., C.M.K., H.V., Z.M., and B.Z. disclose that they are employees of Leyden Laboratories with stock options in this company. B.J. is an advisor to Leyden Laboratories with stock options in this company; J.G. is an advisor to Leyden Laboratories with shares and stock options in this company. Other authors have not reported any conflicts of interest.

Additional information

Supplementary Information The online version contains supplementary material available at https://doi.org/10.1038/s41598-025-94314-5.

Correspondence and requests for materials should be addressed to A.L.B.